IET Communications

The Institution of Engineering and Technology WILEY

ORIGINAL RESEARCH PAPER

Towards the assessment of realistic hybrid precoding in millimeter wave MIMO systems with hardware impairments

Anastasios K. Papazafeiropoulos[1,2] | Georgios K. Papageorgiou[3] | Oluwatayo Y. Kolawole[4] |
Pandelis Kourtessis[1] | Symeon Chatzinotas[2] | John M. Senior[1] | Mathini Sellathurai[3] |
Tharmalingam Ratnarajah[4]

[1] Communications and Intelligent Systems Research Group, University of Hertfordshire, Hatfield, UK

[2] SnT at the University of Luxembourg, Luxembourg

[3] School of Engineering and Physical Sciences, Heriot-Watt University, Edinburgh, UK

[4] Institute for Digital Communications, University of Edinburgh, Edinburgh, UK

Correspondence
Anastasios K. Papazafeiropoulos, University of Hertfordshire, Hatfield AL10 9AB, UK
Email: tapapazaf@gmail.com

Funding information
Fonds National de la Recherche Luxembourg, Grant/Award Numbers: 5G-SKY, ECLECTIC; University of Hertfordshire's 5-year Vice Chancellor's Research Fellowship

Abstract

Hybrid processing in millimeter wave (mmWave) communication has been proposed as a solution to reduce the cost and energy consumption by reducing the number of radio-frequency (RF) chains. However, the impact of the inevitable residual transceiver hardware impairments (RTHIs), including the residual additive transceiver hardware impairments (RATHIs) and the amplified thermal noise (ATN), has not been sufficiently studied in mmWave hybrid processing. In this work, the hybrid precoder and combiner are designed, which include both digital and analog processing by taking into account the RATHIs and the ATN. In particular, a thorough study is provided to shed light on the degradation of the spectral efficiency (SE) of the practical system. The outcomes show the steady degradation of the performance by the ATN across all SNR values, which becomes increasingly critical for higher values of its variance. Furthermore, it is shown that RATHIs result in degradation of the system only in the high SNR regime. Hence, their impact in mmWave system operating at low SNRs might be negligible. Moreover, an increase concerning the number of streams differentiates the impact between the transmit and receive RATHIs with the latter having a more severe effect.

1 | INTRODUCTION

The major identified cornerstones of fifth-generation (5G) communications are millimeter wave (mmWave) transmission, massive multiple-input multiple-output (MIMO) systems, and small cell networks [1]. Specifically, mmWave frequencies have attracted a lot of interest because they can grant large amounts of the unexploited spectrum which could be used for boosting the data rates. In particular, almost 252 GHz of spectrum, found in the interval 30–300 GHz, could be used for mobile broadband [2]. Nevertheless, the high absorption of the wavelengths in mmWave frequencies from all sorts of materials, the short propagating distances, and the low number of established paths between the transmitter and receiver have led to the extensive study of the physical layer in mmWaves [3]. Notably, massive MIMO systems have been proposed as a means to compensate the increased path-losses [1].

Precoding/combining is required for the realization of efficient wireless communication systems as this aids the multiplexing of data streams. Typical sub-6 GHz cellular systems apply entirely digital precoding/combining that operates at the baseband level and requires a single radio frequency (RF) chain per antenna. However, the large number of antennas, suggested by 5G communications, and the hardware constraints significantly increase the cost and power consumption of several components, for example, analog-to-digital converters (ADCs). Therefore, the development of entirely digital precoding/combining mmWave deployments becomes a challenge in practice [4].

One way to address a large number of RF chains is to perform precoding/combining only in the RF domain using analog beamforming. With this approach, phase shifters are used to steer transmit and receive beams along with the propagation directions. Thus, only one RF chain is required to achieve communication. However, analog beamforming is limited by

its inability to perform any form of interference cancellation [5]. Therefore, a hybrid precoding/combining mmWave design has been proposed, which utilizes more RF chains than analog beamforming but much less than the fully digital precoding/combining, providing a good interplay among cost, complexity, and data rate performance [6]. The study of hybrid precoding/combining indicates that two prominent architectures for the implementation of massive MIMO techniques in mmWave networks are the sub-array architecture and the fully connected architecture. In the former, an entire antenna array is divided into sub-arrays, each of which is connected by a phase shifter to one RF chain, whereas, in the latter, each RF chain is coupled with its own phase shifter [5, 7]. In addition, hybrid precoding/combining has been shown to provide near-optimal performance when compared to the digital unconstrained case [6–14]. For example, the authors in [8] considered a hybrid multi-user uplink equalizer but did not model the hardware impairments explicitly as we do in this work while the work in [12] derived a semi-analytic bit error rate expression of a hybrid analog/digital orthogonal frequency-division multiplexing (OFDM) system accounting for the non-linear effects of the power amplifier.

The standard strong assumption among these hybrid precoding works concerning mmWave MIMO communications concerns the use of perfect hardware components. However, in practical applications, the RF front-end (where amplification and down-conversion of signals occur) operates at dynamic ranges of frequencies which are much higher than the operating frequencies of the baseband [15]. On this basis, the signal processing at baseband level cannot remove the residual transceiver hardware impairments (RTHIs) arising from nonlinearities of the amplifier, quantization errors, In-phase/Quadrature (I/Q) imbalance, and mutual coupling between antenna ports [16–18]. Unfortunately, RTHIs present an unavoidable challenge towards the design of commercially attractive mmWave MIMO transceivers. Moreover, massive MIMO systems possibly used for mmWave communication should employ low-quality circuits, which are more susceptible to RTHIs, in order to be a cost-efficient technology [19, 20]. Therefore, the focal point of this paper is to scrutinize the impact of RTHIs on hybrid processing mmWave systems.

In the literature, RTHIs and their impact have been studied extensively in the case of standard well-known massive MIMO systems functioning at lower frequencies, for example, [21–30]. Specifically, residual additive transceiver hardware impairments (RATHIs) and amplified thermal noise (ATN) appear as the two major imperfections [22, 25]. The additive impairments are modelled as power-dependent Gaussian additive noise [23, 27], and results from [27] show that the transmitter distortions have a greater impact than the receive RATHIs. However, in the case of mmWave MIMO systems, only a few works have considered RTHIs in mmWave MIMO systems [31–35]. In [31], the performance of an mmWave system employing analog beamforming under RTHIs is evaluated by using a logarithmic model, which assumes that the combiner losses are only dependent on the number of RF chains. However, analog beamforming is not robust for multi-stream and multi-user scenarios. In [32], although the major RTHIs are studied, the study is based on orthogonal frequency-division multiplexing (OFDM) modulation, while in [33] and [34], digital precoding was assumed to obtain the coverage probability in the realistic case of randomly located base stations. Notably, a first attempt to address the impact of HIs was made in [35], where the authors also considered multiplicative phase noise (PN). However, therein, the SE expression is incorrect. Specifically, we applied the expectation operator to the PN random variable in the SE expression while that was incorrect. We found this mistake recently. Though several attempts were made to find a solution and correct the formula (including the PN), we realized that the existence of an analytical expression for the SE with PN is rather unlikely to exist. Therefore, the presence of PN has been excluded and the formula has now been corrected. Hence, different to previous works, our goal is to provide a more insightful and realistic study for hybrid (not only digital) processing MIMO systems in mmWave frequencies.

1.1 | Motivation and Contribution

The motivation of this work is based on the fact that the majority of existing studies in mmWave communications for 5G networks rely on the common assumption of operating with perfect hardware. While these works have provided valuable insight into the performance of mmWave MIMO systems under various considerations, it is a dire necessity to take into account for RTHIs and assess correctly their effect on mmWave systems before their practical implementation. Thus, taking into consideration the results from [10], which has not accounted for any RTHIs, we develop a general model for the introduction of the RTHIs in mmWave systems, and provide an analysis that will shed light on the realistic potential of hybrid MIMO systems in mmWaves. Notably, the proposed analysis is based on the methodology in [10], but appears to have significant differences, in order to tackle with the presence of RTHIs. In other words, existing results cannot be applied and insightful modifications are required. Moreover, contrary to [35], which includes flaws, we perform a thorough and strict analysis to cover the corresponding literature gap.

Our contributions are summarized as follows:

- We consider a hybrid transceiver with RATHIs and ATN and study their impact on the spectral efficiency (SE) in a point-to-point MIMO communication setup in the mmWave bands. In particular, *we derive a novel expression for the mutual information, which takes into account the considered RTHIs.* To the best of our knowledge, the number of works such as [12] concerning the study of RTHIs in mmWave systems with hybrid precoding is limited.
- We design the hybrid precoders and combiners over practical mmWave MIMO channels with RTHIs by exploiting

the concept of sparse modeling [10], and employ Orthogonal Matching Pursuit (OMP) [36] to solve the corresponding optimization tasks[1]. Moreover, we compare the analytical proposed results to those from spatially sparse hybrid precoding under the impractical assumption of perfect hardware to provide realistic performance and design guidelines of the SE in mmWave MIMO systems.

- We provide extensive simulation results, which highlight the interplay of the key factors of the system with the individual impairments. Especially, we elaborate on the effect of each individual imperfection on the SE. Interestingly, RATHIs result in the degradation of the system performance mostly in the high SNR regime while ATN results in degradation across all SNRs. However, ATN prevails at low SNR values, while RATHIs emerge as more severe at higher SNRs. These conclusions provide important guidelines for design implementation, and show the importance of studying the RTHIs.

The remainder of this paper is organized as follows. Section 2 presents the parameters of the mmWave MIMO system model with hybrid precoding. In Section 3, we provide a description of the various RTHIs under consideration and obtain the SE under their inevitable presence. Next, in Section 4, we provide the hybrid precoder design over practical mmWave MIMO channels with RTHIs. Section 5 presents the numerical results, and Section 6 concludes the paper.

Notation: $\mathcal{B}$, b , $\mathbf{b}$, and $\mathbf{B}$ denote a set, a scalar, a vector, and a matrix, respectively. The notations $\mathbf{B}^{-1}$, $\mathbf{B}^{\mathsf{H}}$, $\mathbf{B}^{T}$ denote the inverse, the Hermitian, and the transpose of matrix $\mathbf{B}$, respectively. Moreover, $(\mathbf{B})_{i,j}$ denotes the entry of matrix $\mathbf{B}$ in the ith row and j^{th} column. The zero vector of length L is denoted as $\mathbf{0}_L$, the zero matrix of dimension $K \times L$ as $\mathbf{O}_{KL}$ and a square zero matrix with K rows/columns is denoted as $\mathbf{O}_K$. Also, tr($\mathbf{B}$) is the trace of $\mathbf{B}$ and $||\mathbf{B}||_F$ expresses the Frobenius norm of $\mathbf{B}$. The notation $\mathbf{b} \sim \mathcal{CN}(\mathbf{0}_N, \boldsymbol{\Sigma})$ denotes a circularly symmetric complex Gaussian vector of length N with zero-mean and covariance matrix $\boldsymbol{\Sigma}$, while $\mathcal{N}(\mathbf{0}_N, \boldsymbol{\Sigma})$ signifies the corresponding real Gaussian variables. Moreover, $\mathbb{E}[\cdot]$ denotes the expectation operator, $\mathbf{I}_N$ is the $N \times N$ identity matrix, and $diag(\mathbf{b})$ creates a diagonal matrix with diagonal entries from the vector $\mathbf{b}$. Finally, $[\mathbf{B}|\mathbf{A}]$ represents horizontal concatenation of matrices with $\mathbf{B}$ and $\mathbf{A}$ having the same row dimension.

2 | SYSTEM MODEL

We begin the analysis with an ideal mmWave MIMO system with hybrid precoding. Then, based on this architecture, we introduce the RATHIs and the ATN, which are inevitable in practical implementations. Hence, we result in a realistic design that is illustrated in Figure 1.

2.1 | Conventional model

A typical mmWave MIMO system is constituted by an M-antenna transmitter communicating with a receiver including N antennas through M_s data streams. Especially, multi-stream communication is allowed in the case that the transmitter consists of M^{F} transmit chains obeying to the constraint $M_s \leq M^{\mathrm{F}} \leq M$. Also, in a hybrid design, the transmitter is composed of a digital baseband precoder, $\mathbf{F}_{\mathrm{B}} \in \mathbb{C}^{M^{\mathrm{F}} \times M_s}$ (with M^{F} transmit chains), and an $M \times M^{\mathrm{F}}$ analog precoder, $\mathbf{F}_{\mathrm{F}}$. The analog precoder, $\mathbf{F}_{\mathrm{F}}$, is implemented by phase shifters. Note that its elements have equal norm satisfying $|(\mathbf{F}_{\mathrm{F}})_{i,j}| = 1/\sqrt{M}$. Thus, the discrete-time transmit signal is expressed by $\mathbf{x} = \mathbf{F}_{\mathrm{F}} \mathbf{F}_{\mathrm{B}} \mathbf{s}$ with $\mathbf{s}$ being the $M_s \times 1$ symbol vector that satisfies $\mathbb{E}[\mathbf{s}\mathbf{s}^{\mathsf{H}}] = \frac{\rho}{M_s}\mathbf{I}_{M_s}$. Concerning the total power constraint of the precoder $\mathbf{F}_{\mathrm{B}}$, it is normalized based on $||\mathbf{F}_{\mathrm{F}} \mathbf{F}_{\mathrm{B}}||_F^2 = M_s$. Taking into account a narrowband[2] block-fading channel model [37], the $N \times 1$ received signal is written as

$$\mathbf{y}_r = \mathbf{H}\mathbf{F}_{\mathrm{F}} \mathbf{F}_{\mathrm{B}} \mathbf{s} + \mathbf{z}, \tag{1}$$

where $\mathbf{H}$ expresses the $N \times M$ channel matrix[3] satisfying $\mathbb{E}[||\mathbf{H}||_F^2] = MN$, while $\mathbf{z}$ expresses the Gaussian noise vector, that is, $\mathbf{z} \sim \mathcal{CN}(0, \sigma^2\mathbf{I}_N)$. Similarly, the receiver includes N^{F} chains and analog shifters obeying to $M_s \leq N^{\mathrm{F}} \leq N$ to process the received signal, which becomes

$$\mathbf{y}_s = \mathbf{W}_{\mathrm{B}}^{\mathsf{H}}\mathbf{W}_{\mathrm{F}}^{\mathsf{H}}\mathbf{H}\mathbf{F}_{\mathrm{F}}\mathbf{F}_{\mathrm{B}}\mathbf{s} + \mathbf{W}_{\mathrm{B}}^{\mathsf{H}}\mathbf{W}_{\mathrm{F}}^{\mathsf{H}}\mathbf{z}, \tag{2}$$

where $\mathbf{W}_{\mathrm{B}}$ denotes the $N^{\mathrm{F}} \times M_s$ baseband digital combining matrix, and $\mathbf{W}_{\mathrm{F}}$ denotes the $N \times N^{\mathrm{F}}$ analog combining matrix that is implemented using phase shifters and obeys $|(\mathbf{W}_{\mathrm{F}})_{i,j}| = 1/\sqrt{N}$.

In the case that the transmission uses Gaussian symbols, the SE of the aforementioned perfect mmWave MIMO channel is expressed as

$$\bar{\mathcal{I}}(\mathbf{F}) = \log_2\left(|\mathbf{I}_{M_s} + \frac{\rho}{M_s}\mathbf{R}^{-1}\mathbf{W}^{\mathsf{H}}\mathbf{H}\mathbf{F}\mathbf{F}^{\mathsf{H}}\mathbf{H}^{\mathsf{H}}\mathbf{W}|\right), \tag{3}$$

where $\mathbf{R} = \sigma^2\mathbf{W}^{\mathsf{H}}\mathbf{W}$ denotes the noise covariance matrix with $\mathbf{W} = \mathbf{W}_{\mathrm{F}}\mathbf{W}_{\mathrm{B}}$ and $\mathbf{F} = \mathbf{F}_{\mathrm{F}}\mathbf{F}_{\mathrm{B}}$ [38].

---

[1] The consideration of RTHIs increases the difficulty and complexity of the hybrid precoding design problem, and we need to reformulate the optimization problem and redesign the optimization algorithm with respect to the ideal case. The presence of RTHIs leads to deviation from the achieved SE reported in [10]. In particular, the channel precoder differs (from the one in [10]) by a multiplicative scalar term, which depends on the RTHIs. As a result, if realistic RTHIs are considered, the SE saturates instead of increasing with the SNR, as it was shown in [10].

[2] Notably, the study of the impact of RTHIs in wideband channels in terms of analytical closed-form results is the topic of the ongoing research.

[3] Implicitly, this model relies on the hypothesis that both the transmitter and receiver are aware of the perfect channel $\mathbf{H}$ because the focus is on the impact of RTHIs and not on the effect of the knowledge of the channel.
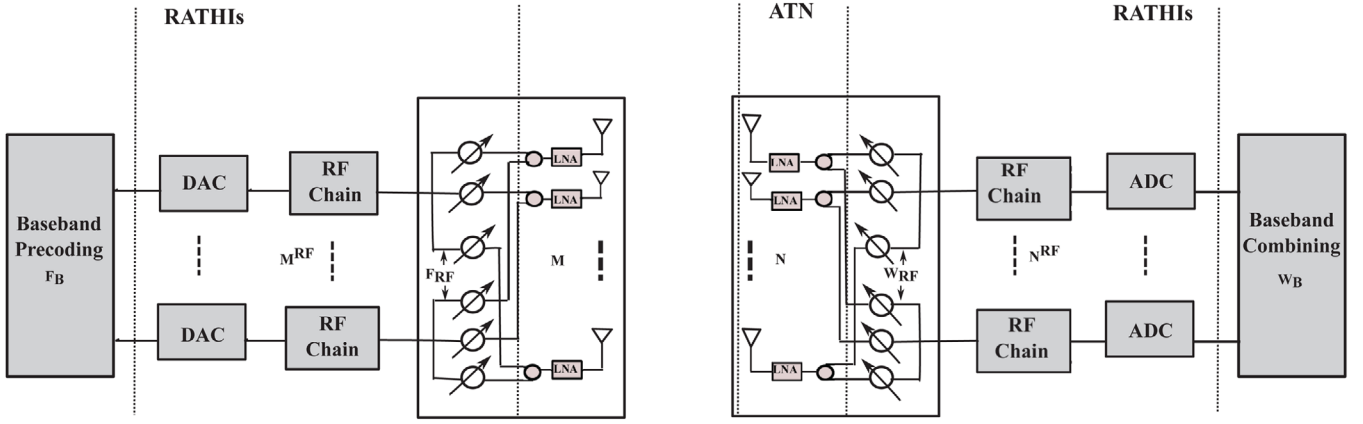
FIGURE 1 A schematic diagram of a realistic hybrid mmWave network with RTHIs

2.2 | Channel characterization

In mmWave communication, the channels experience unique characteristics compared to traditional MIMO systems in sub-6 GHz frequency bands. Specifically, the statistical fading distributions become inaccurate because of: (i) the spatial selectivity, (ii) the high path-loss, and (iii) the increased antenna correlation, since mmWave transceivers are cost efficient when their antenna arrays are very densely collocated. With these characteristics, the extended Saleh–Valenzuela model to mmWave MIMO channels [39, 40] enables us to describe mathematically the mmWave MIMO channel by a narrowband clustered channel in poor scattering environment characteristics as[4]

$$\mathbf{H} = \sqrt{\frac{MN}{L}} \sum_{l=1}^{L} \alpha_l \mathbf{a}_r(\phi_l) \mathbf{a}_t^{\mathsf{H}}(\theta_l), \qquad (4)$$

where L expresses the average path loss between the transmitter and the receiver, and α_l denotes the complex gain of the [th] path assumed to follow the Rayleigh distribution. In other words, $\alpha_l \sim \mathcal{CN}(0, \bar{a})$ with $l = 1, \ldots, L$ and $\bar{a}$ being the average power gain. Given that our motivation is to focus on the impact of RTHIs, we consider only 2D (horizontal) beamforming at both the transmitter and the receiver. Hence, the variables $\theta_l \in [0, 2\pi]$ and $\phi_l \in [0, 2\pi]$ correspond to the l path of the azimuth angles of departure and arrival (AoDs/AoAs) of the transmitter and receiver, respectively. Similarly, the corresponding antenna array response and steering vectors are described by $\mathbf{a}_r(\phi_l)$ and $\mathbf{a}_t(\theta_l)$, respectively. Although the results obtained in this paper can be considered for arbitrary antenna deployments, in this work we assume uniform linear arrays (ULAs). Hence, the array steering vector of the transmitter is written as

$$\mathbf{a}_t(\theta_l) = \frac{1}{\sqrt{M}} \left[1, e^{j\frac{2\pi}{\lambda} d \sin(\theta_l)}, \ldots, e^{j\frac{2(M-1)\pi}{\lambda} d \sin(\theta_l)} \right]^T, \quad (5)$$

where λ and d denote the wavelength and distance between the antenna elements, respectively. Similarly, the response vector at the receiver is expressed as

$$\mathbf{a}_r(\phi_l) = \frac{1}{\sqrt{N}} \left[1, e^{j\frac{2\pi}{\lambda} d \sin(\phi_l)}, \ldots, e^{j\frac{2(N-1)\pi}{\lambda} d \sin(\phi_l)} \right]^T. \quad (6)$$

3 | RTHIs IN HYBRID PROCESSING

In practice, the hybrid transceiver of a MIMO system depends on various residual impairments as depicted by Figure 1. Next, we present these impairments in terms of their models which can be described both physically and mathematically. Specifically, we focus on: (a) the residual additive power-dependent imperfections at the transmitter and receiver, and (b) the ATN at the receiver side.

3.1 | RATHIs

One inevitable category of RTHIs includes the RATHIs that result from the antenna coupling, I/Q mismatch, and the quantization noise in the Digital-to-Analog Converters (DACs) at the transmitter and the Analog-to-Digital Converters (ADCs) at the receiver, Also, RATHIs approximate generic non-linearities, and the leakage between subcarriers due to calibration error [15], [41, Ch. 14]. Especially, the distortions at the transmitter take place from a discrepancy between the signal to be transmitted and the generated signal. Similarly, the reception processing at the receiver includes the distortion of the received signal. Notably, these impairments are expressed in terms of additive random variables in the signal model.

Concerning the mathematical representation of RATHIs, we denote $\mathbf{Q}$ being the transmit covariance matrix having diagonal elements $q_1, \ldots, q_M$. Measurement results suggest that the additive transmitter and receiver distortion noises can be described by random variables that follow circularly symmetric complex Gaussian distributions with average power analogous to the

---

[4] From the physical aspect, it expresses a geometric model with L scatterers, where each scatterer is assumed to contribute a single propagation path.

signal power [16, 18]. From the physical point of view, the Gaussianity can be motivated analytically by the central limit theorem, where the distortion noise describes the aggregation of the contributions from a large number of impairments [15, 19]. Mathematically, the additive imperfections at the transmit and the receive sides are described by

$$\boldsymbol{\eta}_t \sim \mathcal{CN}(\mathbf{0}_M, \boldsymbol{\Lambda}), \tag{7}$$

$$\boldsymbol{\eta}_r \sim \mathcal{CN}(\mathbf{0}_N, \boldsymbol{\Upsilon}), \tag{8}$$

where $\boldsymbol{\Lambda} = \kappa_t^2 \operatorname{diag}\{q_1, \dots, q_M\}$ and $\boldsymbol{\Upsilon} = \kappa_r^2 \mathbf{HQH}^{\mathsf{H}}$. When $\kappa_t = \kappa_r = 0$, we result in the ideal model.

3.2 | ATN

The amplified thermal noise has an impact only on the receiver, and it is described by an increase in the variance of the thermal noise due to an amplification of the thermal noise by receiver components such as the low noise amplifiers and mixers in the receiver hardware and interference leakage from other frequency bands [20]. Hence, the total ATN effect, $\boldsymbol{\xi}$, is described by a complex Gaussian distribution with zero mean and variance $\sigma_\xi^2 \mathbf{I}_N$ satisfying $\sigma^2 \leq \sigma_\xi^2$, where σ^2 expresses the parameter of the actual thermal noise. Notably, the thermal noise is time-dependent because it results from samples taken from a white noise process passed through an amplified "filter".

3.3 | Hybrid processing with RTHIs

Inserting the RTHIs into the analysis, the received signal is written as

$$\widetilde{\mathbf{y}}_s = \mathbf{W}_{\mathrm{B}}^{\mathsf{H}} \mathbf{W}_{\mathrm{F}}^{\mathsf{H}} \mathbf{H}(\mathbf{F}_{\mathrm{F}} \mathbf{F}_{\mathrm{B}} \mathbf{s} + \boldsymbol{\eta}_t) + \mathbf{W}_{\mathrm{B}}^{\mathsf{H}} \mathbf{W}_{\mathrm{F}}^{\mathsf{H}}(\boldsymbol{\eta}_r + \boldsymbol{\xi})$$

$$= \mathbf{W}^{\mathsf{H}} \mathbf{HFs} + \mathbf{W}^{\mathsf{H}} \mathbf{e}, \tag{9}$$

where $\mathbf{F} = \mathbf{F}_{\mathrm{F}} \mathbf{F}_{\mathrm{B}}$, $\mathbf{W} = \mathbf{W}_{\mathrm{F}} \mathbf{W}_{\mathrm{B}}$ and $\mathbf{e} = \mathbf{H}\boldsymbol{\eta}_t + \boldsymbol{\eta}_r + \boldsymbol{\xi}$. Equation (9) differs from (2) in terms of the RATHIs incorporated at the transmitter and receiver, that is, by means of $\boldsymbol{\eta}_t$ and $\boldsymbol{\eta}_r$, while we have also included the ATN at the receiver side through $\boldsymbol{\xi}$[5]. Specifically, in our setting, we have

$$\boldsymbol{\eta}_t \sim \mathcal{CN}\left(\mathbf{0}_M, \kappa_t^2 \frac{\rho}{M_s} \mathbf{I}_M\right), \tag{10}$$

$$\boldsymbol{\eta}_r \sim \mathcal{CN}\left(\mathbf{0}_N, \kappa_r^2 \rho \mathbf{HH}^{\mathsf{H}}\right), \tag{11}$$

where κ_t^2 and κ_r^2 are proportionality constants expressing the severity of the RATHIs at both sides of the system, respectively.

---

[5] Although the considered RTHIs describe indirectly the nonlinearities of the power amplifiers, their critical role in mmWave transmission could result in a future work providing an in-depth study by applying the model in [12].

Notably, each one of the RATHIs corresponds to the ratio of the additive distortion noise variance over the signal power, and in practical systems, they are known as Error Vector Magnitudes (EVMs) of the transceiver [41].

Lemma 1. *The SE of an mmWave MIMO system with RATHIs and ATN is expressed as*

$$SE = \log_2\left(\left|\mathbf{I}_{M_s} + \frac{\rho}{M_s} \widetilde{\mathbf{R}}^{-1} \mathbf{W}^{\mathsf{H}} \mathbf{HFF}^{\mathsf{H}} \mathbf{H}^{\mathsf{H}} \mathbf{W}\right|\right), \tag{12}$$

where $\widetilde{\mathbf{R}} = \mathbf{W}^{\mathsf{H}} \mathbf{R}_{\mathrm{e}} \mathbf{W}$ and

$$\mathbf{R}_{\mathrm{e}} = \mathbb{E}\{\mathbf{ee}^{\mathsf{H}}\}$$

$$= \left(\kappa_t^2 \frac{\rho}{M_s} + \kappa_r^2 \rho\right) \mathbf{HH}^{\mathsf{H}} + \sigma_\xi^2 \mathbf{I}_N. \tag{13}$$

Proof. Please see Appendix A. □

According to Lemma 1, we observe that the impact of RTHIs is hidden in the covariance matrix, thus, degrading the SE. In addition, a clear dependence with the transmit power and the number of data streams is shown.

4 | SPATIALLY SPARSE PRECODING FOR AN mmWave MIMO CHANNEL WITH RTHIs

The focus of this section concerns the maximization of the SE described by (12) by means of the appropriate design of the hybrid mmWave precoders ($\mathbf{F}_{\mathrm{F}}, \mathbf{F}_{\mathrm{B}}$) and the hybrid mmWave combiners ($\mathbf{W}_{\mathrm{F}}, \mathbf{W}_{\mathrm{B}}$). The maximization demands for the joint optimization of four matrix variables being the mmWave precoders and combiners with non-convex constraints on $\mathbf{F}_{\mathrm{F}}$ and $\mathbf{W}_{\mathrm{F}}$. It is well known that an exact solution is not possible to be obtained due to the intractability of the corresponding problem [42]. Hence, we address this issue by following a method similar to [10], where the joint precoder-combiner optimization was decoupled. However, the proposed analysis, including the RTHIs, requires different manipulations, being insightful at the same time. For instance, the authors in [10] employed a compact SVD (based on the rank of the channel matrix) for their analysis. In our case, the decomposition of the channel matrix requires a different approach. In particular, we used the full SVD, which is required for the factorization of the matrix in (13). Hence, we distinguished between two cases $N \geq M$ and $N < M$ for the analysis purposes.

4.1 | Hybrid precoder design for an mmWave MIMO transmitter with RTHIs

Having as a focal point the optimization of the SE, we start by designing the hybrid precoders ($\mathbf{F}_{\mathrm{F}}, \mathbf{F}_{\mathrm{B}}$) that maximize the mutual information of a practical mmWave MIMO channel with

RTHIs by means of Gaussian signaling. We rely on the assumption that the receiver can achieve optimal nearest-neighbour decoding of the received signal, $\widetilde{\mathbf{y}}_r$ [10]. Thus, the mutual information is provided by

$$\mathcal{I}(\mathbf{F}) = \log_2\left(\left|\mathbf{I}_N + \frac{\rho}{M_s}\mathbf{R}_e^{-1}\mathbf{H}\mathbf{F}\mathbf{F}^H\mathbf{H}^H\right|\right), \qquad (14)$$

where

$$\widetilde{\mathbf{y}}_r = \mathbf{H}(\mathbf{F}_F\mathbf{F}_B\mathbf{s} + \boldsymbol{\eta}_t) + \boldsymbol{\eta}_r + \boldsymbol{\xi}. \qquad (15)$$

The assumption that the receiver is aware of the received signal $\mathbf{y}_r$ to perform optimal nearest-neighbor decoding is not realistic in practice. Therefore, the received signals should be combined before decoding. The design of the mmWave hybrid combiners in the analog and digital domains will be examined in a subsequent section.

The optimization problem, providing the precoders $\mathbf{F}_F$, $\mathbf{F}_B$, takes the form

$$\mathcal{P}_1 : (\mathbf{F}_F^{\mathrm{opt}}, \mathbf{F}_B^{\mathrm{opt}}) = \underset{\mathbf{F}_F, \mathbf{F}_B}{\arg\max} \ \mathcal{I}(\mathbf{F})$$

$$\text{s.t. } \mathbf{F}_F \in \mathcal{F}_F,$$

$$||\mathbf{F}||_F^2 = M_s, \qquad (16)$$

with $\mathcal{F}_F$ expressing the set of $M \times M^F$ matrices which represent the feasible F precoders with constant-magnitude entries[6]. Given the non-convexity of the constraint $\mathbf{F}_F \in \mathcal{F}_F$, no general solutions exist. For this reason, we reformulate (16), in order to obtain near-optimal precoders that can be constructed in practical applications.

Firstly, we consider the use of Singular Value Decomposition (SVD) to the channel matrix $\mathbf{H}$, that is, $\mathbf{H} = \mathbf{U}\boldsymbol{\Sigma}\mathbf{V}^H$, where $\mathbf{U}$ and $\mathbf{V}$ are $N \times N$ and $M \times M$ unitary matrices, respectively. Also, $\boldsymbol{\Sigma}$ is an $N \times M$ matrix consisting of singular values on its main diagonal in decreasing order. To this end, the matrix $\mathbf{R}_e$ can be decomposed as $\mathbf{R}_e = \mathbf{U}\mathbf{D}\mathbf{U}^H$, where

$$\mathbf{D} = \beta\boldsymbol{\Sigma}\boldsymbol{\Sigma}^T + \sigma_\xi^2\mathbf{I}_N, \qquad (17)$$

and $\beta = \frac{\kappa_t^2\rho}{M_s} + \kappa_r^2\rho$. Hence, after several algebraic manipulations and using the Sylvester's determinant identity, the mutual information in (14) yields

$$\mathcal{I}(\mathbf{F}) = \log_2\left(\left|\mathbf{I}_M + \frac{\rho}{M_s}\boldsymbol{\Sigma}^T\mathbf{D}^{-1}\boldsymbol{\Sigma}V^H\mathbf{F}\mathbf{F}^H\mathbf{V}\right|\right). \qquad (18)$$

Next, we write the matrices $\boldsymbol{\Sigma}$ and $\mathbf{V}$ for the case where $N \geq M$ as

$$\boldsymbol{\Sigma} = \begin{bmatrix} \boldsymbol{\Sigma}_1 & \mathbf{O}_{M_s,K} \\ \mathbf{O}_{K,M_s} & \boldsymbol{\Sigma}_2 \\ \mathbf{O}_{L,M_s} & \mathbf{O}_{L,K} \end{bmatrix}, \ \mathbf{V} = [\mathbf{V}_1 \ \mathbf{V}_2], \qquad (19)$$

where $\boldsymbol{\Sigma}_1$ is of dimension $M_s \times M_s$ (with the M_s largest singular values of the channel matrix), and $\boldsymbol{\Sigma}_2$ is $K \times K$ with $K = M - M_s$ and $L = N - M$. Note that the matrices $\mathbf{V}_1$ and $\mathbf{V}_2$ are $M \times M_s$ and $M \times K$, respectively. In particular, the optimal precoder for $\mathbf{H}$ with no constraints is $\mathbf{F}^{\mathrm{opt}} = \mathbf{V}_1$. Given that the optimal precoder $\mathbf{V}_1$ cannot be expressed by means of $\mathbf{F}$, we are approaching the optimal $\mathbf{V}_1$ so that the mutual information corresponding to $\mathbf{V}_1\mathbf{F}$ (or $\mathbf{V}_1^H\mathbf{F}$) is approximately equivalent.

Remark 1. The difference to the ideal case, which is one of the major contributions of this work, is that by considering the RTHIs in a practical scenario the optimal precoder cannot be realized anymore, as we will present next. Specifically, we should note that in [10] the authors used the compact SVD (which is more economical), yielding a diagonal $\boldsymbol{\Sigma}$ matrix of dimension $\mathrm{rank}(\mathbf{H}) \times \mathrm{rank}(\mathbf{H})$. However, in our analysis the full SVD is required for the decomposition of $\mathbf{R}_e$ and derivation of $\mathbf{D}$ as in (17), which leads to (18).

Assumption 1. The parameters of the mmWave MIMO system define the hybrid precoder close to the optimal unitary precoder $\mathbf{V}_1$. Specifically, the mathematical conditions necessitate $\mathbf{V}_1^H\mathbf{F} \approx \mathbf{I}_{M_s}$, or equivalently, the matrix $\mathbf{I}_{M_s} - \mathbf{V}_1^H\mathbf{F}\mathbf{F}^H\mathbf{V}_1 \approx \mathbf{O}_{M_s}$, that is, to be small. Additionally, $\mathbf{V}_2^H\mathbf{F} \approx \mathbf{O}_{KM_s}$ holds, which alternatively states that the singular values of $\mathbf{V}_2\mathbf{F}$ are small.[7]

Making use of the partition in (19), the term $\mathbf{V}^H\mathbf{F}\mathbf{F}^H\mathbf{V}$ in (18) can be expressed as

$$\mathbf{V}^H\mathbf{F}\mathbf{F}^H\mathbf{V} = \begin{bmatrix} \mathbf{V}_1^H\mathbf{F}\mathbf{F}^H\mathbf{V}_1 & \mathbf{V}_1^H\mathbf{F}\mathbf{F}^H\mathbf{V}_2 \\ \mathbf{V}_2^H\mathbf{F}\mathbf{F}^H\mathbf{V}_1 & \mathbf{V}_2^H\mathbf{F}\mathbf{F}^H\mathbf{V}_2 \end{bmatrix}$$

$$= \begin{bmatrix} \mathbf{A}_{11} & \mathbf{A}_{12} \\ \mathbf{A}_{21} & \mathbf{A}_{22} \end{bmatrix}. \qquad (20)$$

We also have

$$\mathbf{D} = \begin{bmatrix} \beta\boldsymbol{\Sigma}_1^2 + \sigma_\xi^2\mathbf{I}_{M_s} & \mathbf{O}_{M_s,K} & \mathbf{O}_{M_s,L} \\ \mathbf{O}_{K,M_s} & \beta\boldsymbol{\Sigma}_2^2 + \sigma_\xi^2\mathbf{I}_K & \mathbf{O}_{KL} \\ \mathbf{O}_{L,M_s} & \mathbf{O}_{L,K} & \sigma_\xi^2\mathbf{I}_L \end{bmatrix}, \qquad (21)$$

which can be used for the calculation of the following matrix product

$$\mathbf{B} = \frac{\rho}{M_s}\boldsymbol{\Sigma}^T\mathbf{D}^{-1}\boldsymbol{\Sigma} \qquad (22)$$

$$= \begin{bmatrix} \mathbf{B}_1 & \mathbf{O}_{M_s,K} \\ \mathbf{O}_{KM_s} & \mathbf{B}_2 \end{bmatrix}, \qquad (23)$$

---

[6] Contrary to [10], the optimization problem includes the RTHIs.

[7] These approximations are expected to be tight in the system conditions under investigation including a large number of transmit antennas, correlated channels, and transmit chains $M_s < M^F \leq M$.

where

$$\mathbf{B}_1 = (\rho/M_s)\boldsymbol{\Sigma}_1^2(\beta\boldsymbol{\Sigma}_1^2 + \sigma_\xi^2\mathbf{I}_{M_s})^{-1}, \tag{24}$$

$$\mathbf{B}_2 = (\rho/M_s)\boldsymbol{\Sigma}_2^2(\beta\boldsymbol{\Sigma}_2^2 + \sigma_\xi^2\mathbf{I}_K)^{-1}. \tag{25}$$

The inversion of $\mathbf{D}$ is straightforward, since it is a diagonal matrix. Taking (19)–(25) into account, the mutual information can be simplified to

$$\mathcal{I}(\mathbf{F}) = \log_2\left(\left|\mathbf{I}_M + \begin{bmatrix} \mathbf{B}_1 & \mathbf{O}_{M_s,K} \\ \mathbf{O}_{KM_s} & \mathbf{B}_2 \end{bmatrix} \begin{bmatrix} \mathbf{A}_{11} & \mathbf{A}_{12} \\ \mathbf{A}_{21} & \mathbf{A}_{22} \end{bmatrix}\right|\right)$$

$$\overset{(a)}{=} \log_2\left(\left|\mathbf{I}_{M_s} + \mathbf{B}_1\mathbf{A}_{11}\right|\right) + \log_2\left(\left|\mathbf{I}_K + \mathbf{B}_2\mathbf{A}_{22}\right.\right.$$

$$\left.\left. - \mathbf{B}_2\mathbf{A}_{21}\left(\mathbf{I}_{M_s} + \mathbf{B}_1\mathbf{A}_{11}\right)^{-1}\mathbf{B}_1\mathbf{A}_{12}\right|\right)$$

$$\overset{(b)}{\approx} \log_2\left(\left|\mathbf{I}_{M_s} + \mathbf{B}_1\mathbf{V}_1^H\mathbf{F}\mathbf{F}^H\mathbf{V}_1\right|\right), \tag{26}$$

where in (a) we have employed the identity for determinants regarding the Schur complement, and (b) results from Assumption 1 that $\mathbf{A}_{12}$, $\mathbf{A}_{21}$, and $\mathbf{A}_{22}$ are approximately equal to zero. The elements of the diagonal matrix $\mathbf{B}_1$ are given by

$$(\mathbf{B}_1)_{i,i} = \frac{\frac{\rho}{M_s}\sigma_1^2(i)}{\beta\sigma_1^2(i) + \sigma_\xi^2}$$

$$= \frac{\sigma_1^2(i)}{\left(\kappa_t^2 + M_s\kappa_r^2\right)\sigma_1^2(i) + M_s/\bar{\rho}}, \tag{27}$$

where $\bar{\rho} = \rho/\sigma_\xi^2$ denotes the SNR and $\sigma_1(i)$ is the ith singular value of the partitioned $\boldsymbol{\Sigma}$, that is, $\boldsymbol{\Sigma}_1$. Further manipulations to (26) enable its simplification to

$$\mathcal{I}(\mathbf{F}) \overset{(a)}{\approx} \log_2\left(\left|\mathbf{I}_{M_s} + \mathbf{B}_1\right|\right) + \log_2\left(\left|\mathbf{I}_{M_s} - \right.\right.$$

$$\left.\left(\mathbf{I}_{M_s} + \mathbf{B}_1\right)^{-1}\mathbf{B}_1\left(\mathbf{I}_{M_s} - \mathbf{V}_1^H\mathbf{F}\mathbf{F}^H\mathbf{V}_1\right)\right|\right)$$

$$\overset{(b)}{\approx} \log_2\left(\left|\mathbf{I}_{M_s} + \mathbf{B}_1\right|\right) - \mathrm{tr}\left(\left(\mathbf{I}_{M_s} + \mathbf{B}_1\right)^{-1}\right.$$

$$\left. \times\mathbf{B}_1\left(\mathbf{I}_{M_s} - \mathbf{V}_1^H\mathbf{F}\mathbf{F}^H\mathbf{V}_1\right)\right)$$

$$\overset{(c)}{\approx} \log_2\left(\left|\mathbf{I}_{M_s} + \mathbf{B}_1\right|\right) - \beta\mathrm{tr}\left(\mathbf{I}_{M_s} - \mathbf{V}_1^H\mathbf{F}\mathbf{F}^H\mathbf{V}_1\right)$$

$$= \log_2\left(\left|\mathbf{I}_{M_s} + \mathbf{B}_1\right|\right) - \beta M_s + \|\widetilde{\mathbf{V}}_1^H\mathbf{F}\|_F^2, \tag{28}$$

where in (a) we have applied the identity $\mathbf{I} + \mathbf{B}_1\mathbf{A}_{11} = (\mathbf{I} + \mathbf{B}_1)(\mathbf{I} - (\mathbf{I} + \mathbf{B}_1)^{-1}\mathbf{B}_1(\mathbf{I} - \mathbf{A}_{11}))$; (b) follows from Assumption 1, because the eigenvalues of matrix $\mathbf{C} = (\mathbf{I}_{M_s} + \mathbf{B}_1)^{-1}\mathbf{B}_1(\mathbf{I}_{M_s} - \mathbf{V}_1^H\mathbf{F}\mathbf{F}^H\mathbf{V}_1)$ are small leading to the approximation $\log_2(|\mathbf{I}_{M_s} - \mathbf{C}|) \approx \log_2(1 - \mathrm{tr}(\mathbf{C})) \approx -\mathrm{tr}(\mathbf{C})$; (c) is derived by using the high SNR approximation

$$\lim_{\bar{\rho}\to\infty}\left(\mathbf{I}_{M_s} + \mathbf{B}_1\right)^{-1}\mathbf{B}_1 = \beta\mathbf{I}_{M_s}, \tag{29}$$

where $\beta = \kappa_t^2 + M_s\kappa_r^2$ and

$$\widetilde{\mathbf{V}}_1 = \sqrt{\gamma}\mathbf{V}_1, \tag{30}$$

with $\gamma = (\beta + 1)^{-1}$, which concludes the analysis. Note that we have replaced the chordal distance by the Euclidean distance by exploiting the manifold's locally Euclidean property since Approximation 1 denotes the closeness between these two points.

The analysis for the case where $N < M$ is similar and for brevity is presented in Appendix B.

Remark 2. The difference with respect to the ideal (impractical) scenario provided by [10] can be clearly seen by means of β, $\mathbf{B}_1$, and $\widetilde{\mathbf{V}}_1$, which include the impact of RTHIs.

Remark 3. From (30), we observe that in the case of ideal hardware, where no RATHIs ($\kappa_t^2 = \kappa_r^2 = 0$) and insignificant amplified thermal noise occur, the expression for the mutual information (28) coincides with [10] since $\gamma = 1$. However, in practice both terms κ_t^2 and κ_r^2 are non-zero leading to a degradation in the mutual information of the system, as we will demonstrate in Section 5.

Obviously, a closer look at the third term of (28) reveals that if $\mathbf{F}$ was unitary, it would express the squared chordal distance between $\widetilde{\mathbf{V}}_1$ and $\mathbf{F}$, which is represented by two points on the Grassmanian manifold. Based on Assumption 1, we are qualified to substitute the chordal distance by the Euclidean distance given by $\|\widetilde{\mathbf{V}}_1 - \mathbf{F}\|_F$. This is quite useful, since it serves our aim to maximize $\mathcal{I}(\mathbf{F})$. Thus, our focal point will be the maximization of $\mathrm{tr}(\widetilde{\mathbf{V}}_1^H\mathbf{F})$ instead of $\|\widetilde{\mathbf{V}}_1 - \mathbf{F}\|_F^2$, bearing in mind their equivalence due to the assumption (see [10] for more details). Thus, the optimization problem in (16) can be rewritten as

$$\mathcal{P}_2 : (\mathbf{F}_F^{\mathrm{opt}}, \mathbf{F}_B^{\mathrm{opt}}) = \underset{\mathbf{F}_F,\mathbf{F}_B}{\arg\min} \quad \|\widetilde{\mathbf{V}}_1 - \mathbf{F}_F\mathbf{F}_B\|_F$$

$$\text{s.t.} \quad \mathbf{F}_F \in \mathcal{F}_F \tag{31}$$

$$\|\mathbf{F}_F\mathbf{F}_B\|_F^2 = M_s.$$

In other words, the task is to find the projection of a scaled version of $\widetilde{\mathbf{V}}_1$, onto the set of precoders having the form of $\mathbf{F} = \mathbf{F}_F\mathbf{F}_B$ with $\mathbf{F}_F$ belonging to the set of $\mathcal{F}_F$. Note that this

projection takes place by means of the standard Frobenius term. However, finding the projection in closed form presents an algorithmic intractability due to the non-convexity introduced by the set $\mathcal{F}_F$ [43, 44].

Exploiting the properties of the mmWave MIMO channel, we result in a near-optimal solution of (31) by certain observations. Specifically, (1) an orthonormal basis regarding the row space of the channel is formed by the columns of the unitary matrix $\mathbf{V}$, (2) a basis is formed for the same space by the linearly independent array response vectors $\mathbf{a}_t(\theta_l)$, (3) as a consequence of properties (1), and (2), the optimal precoder $\widetilde{\mathbf{V}}_1$ can be expressed as a linear combination of vectors $\mathbf{a}_t(\theta_l)$, and (4) since $\mathbf{a}_t(\theta_l)$ are constant-magnitude phase-only vectors that can be implemented at RF using analog phase shifters, the mmWave transmitter can employ M^F of the vectors $\mathbf{a}_t(\theta_l)$ and define arbitrary linear combinations of $\mathbf{a}_t(\theta_l)$ by using the digital precoder $\mathbf{F}_B$. As a result, a linear combination, minimizing $||\widetilde{\mathbf{V}}_1 - \mathbf{F}||_F$, can be constructed. Hence, the optimization problem $\mathcal{P}_2$ can be formulated by accounting for the restriction on the set $\mathcal{F}_F$ to $\mathbf{a}_t(\theta_l)$. In fact, we have

$$\mathcal{P}_3 : (\mathbf{F}_F^{opt}, \mathbf{F}_B^{opt}) = \underset{\mathbf{F}_F, \mathbf{F}_B}{\arg\min} \quad ||\widetilde{\mathbf{V}}_1 - \mathbf{F}_F \mathbf{F}_B||_F$$

$$\text{s.t.} \quad \mathbf{F}_F^{(l)} \in \{\mathbf{a}_t(\theta_l), \forall l\} \quad (32)$$

$$||\mathbf{F}_F \mathbf{F}_B||_F^2 = M_s.$$

The purpose of $\mathcal{P}_3$ is to find the optimal low dimensional representation of $\widetilde{\mathbf{V}}_1$ in terms of the optimal basis formed by $\mathbf{a}_t(\theta_l)$. Embedding $\mathbf{F}_F^{(l)}$ into the optimization objective, we lead to

$$\mathcal{P}_4 : (\widetilde{\mathbf{F}}_B^{opt}) = \underset{\widetilde{\mathbf{F}}_B}{\arg\min} ||\widetilde{\mathbf{V}}_1 - \mathbf{A}_t \widetilde{\mathbf{F}}_B||_F$$

$$\text{s.t.} \quad ||\text{diag}(\widetilde{\mathbf{F}}_B \widetilde{\mathbf{F}}_B^H)||_0 = M^F \quad (33)$$

$$||\mathbf{A}_t \widetilde{\mathbf{F}}_B||_F^2 = M_s,$$

where $\mathbf{A}_t = [\mathbf{a}_t(\theta_1), \dots, \mathbf{a}_t(\theta_L)]$ is an $M \times L$ matrix containing the array response vectors, while $\widetilde{\mathbf{F}}_B$ is an $L \times M_s$ matrix.

The roles of matrices $\mathbf{A}_t$ and $\widetilde{\mathbf{F}}_B$ in obtaining $\mathbf{F}_F^{opt}$ and $\mathbf{F}_B^{opt}$ are auxiliary as far as the sparsity constraint $||\text{diag}(\widetilde{\mathbf{F}}_B \widetilde{\mathbf{F}}_B^H)||_0 = M^F$ is concerned. This suggests that $\widetilde{\mathbf{F}}_B$ cannot have more than M^F non-zero rows. Actually, when $\widetilde{\mathbf{F}}_B$ includes exactly M^F non-zero rows, M^F columns of $\mathbf{A}_t$ are chosen. In such a case, the baseband precoder, $\mathbf{F}_B^{opt}$ and the RF precoder, $\mathbf{F}_F^{opt}$ will be obtained by M^F non-zero rows of $\widetilde{\mathbf{F}}_B$ and the corresponding columns of $\mathbf{A}_t$, respectively.

The problem described by (33) is analogous to approximation problems for signal recovery by multiple measurement vectors [36, 45, 46]. Based on the OMP method [36], we amend the pseudo-code describing the precoder in [10], in order to consider the RTHIs. Specifically, we introduce Algorithm 1, resulting in the precoder solution. First, we find the vector $\mathbf{a}_t(\theta_l)$, which is more correlated to the residual $\mathbf{F}_{res}$ in Step 6. The

ALGORITHM 1 Spatially Sparse Precoding with RATHIs by OMP

1   **Require** $\widetilde{\mathbf{V}}_1$

2    $\mathbf{F}_F = $ Empty Matrix

3    $\mathbf{F}_{res} = \widetilde{\mathbf{V}}_1$

4   **for** $i \leq M^F$ **do**

5      $\boldsymbol{\Psi} = \mathbf{A}_t^H \mathbf{F}_{res}$

6      $k = \underset{l=1,\dots,L}{\arg\max} (\boldsymbol{\Psi}\boldsymbol{\Psi}^H)_{l,l}$

7      $\mathbf{F}_F = [\mathbf{F}_F | \mathbf{A}_t^{(k)}]$

8      $\mathbf{F}_B = (\mathbf{F}_F^H \mathbf{F}_F)^{-1} \mathbf{F}_F^H \widetilde{\mathbf{V}}_1$

9      $\mathbf{F}_{res} = \frac{\widetilde{\mathbf{V}}_1 - \mathbf{F}_F \mathbf{F}_B}{||\widetilde{\mathbf{V}}_1 - \mathbf{F}_F \mathbf{F}_B||_F}$

10   **end**

11    $\mathbf{F}_B = \sqrt{M_s} \frac{\mathbf{F}_B}{||\mathbf{F}_F \mathbf{F}_B||_F}$

12   **return** $\mathbf{F}_F, \mathbf{F}_B$

optimal precoder $\widetilde{\mathbf{V}}_1$ obtains its maximum projection in the direction of this vector. Next, Step 8 describes the least-squares solution to $\mathbf{F}_B$ in an OMP fashion, that is, on the restricted set of columns included in the matrix $\mathbf{F}_F$. The selection of the M^F beamforming vectors will require M^F iterations. Then, the construction of the precoding matrix $\mathbf{F}_F$ will have taken place, and the optimal baseband precoder $\mathbf{F}_B$ will have been obtained.

Remark 4. The difference to the OMP algorithm used in sparse precoding is that of a scaling factor in the optimal solution V_1, leading to a suboptimal precoder $\widetilde{V}_1$. In the presence of hardware impairments, $\widetilde{V}_1$ will be the best possible precoder that can be approximated/solved by any method (not just OMP).

4.2 | Hybrid combiner design for an mmWave MIMO receiver with RTHIs

This section focuses on the practical design of the combiners in both analog and digital domains. Given that the realistic receivers will combine the received signals before detection, we concentrate in the design of the hybrid combiners $(\mathbf{W}_F, \mathbf{W}_B)$ to ensure the minimization of the mean squared error (MSE) between the transmit and receive signals in a realistic mmWave MIMO channel with RTHIs.

Hence, the combiners $(\mathbf{W}_F, \mathbf{W}_B)$ will be provided by means of the optimization problem, taking the form

$$\mathcal{R}_1 : (\mathbf{W}_F^{opt}, \mathbf{W}_B^{opt}) = \underset{\mathbf{W}_F, \mathbf{W}_B}{\arg\min} \mathbb{E}\left[||\mathbf{s} - \mathbf{W}^H \mathbf{y}_r||_2^2\right],$$

$$\text{s.t.} \quad \mathbf{W}_F \in \mathcal{W}_F, \quad (34)$$

where $\mathcal{W}_F$ denotes the set of $N \times N^F$ matrices describing the feasible F combiners, and having constant-gain entries. In this case, we consider the optimal precoders, $(\mathbf{F}_F^{opt}, \mathbf{F}_B^{opt})$ to be fixed

since they have been determined by the transmitter. Analogous to the precoder design, no general solutions are known to (34) because of the non-convex constraint, $\mathbf{W}_{\mathrm{F}} \in \mathcal{W}_{\mathrm{F}}$. Interestingly, an exact solution to the MSE optimization problem in (34) would have been possible with the implementation of matrix inversion lemma as in [10, 47] without hardware impairments. For such a case, we suggest an approximation of (34) enabling us to obtain the optimal combiners minimizing the MSE between the transmit and receive signals. The method follows similar steps with those used in solving constrained minimum MSE (MMSE) problems in [48]. First, we rewrite the objective function of (34) that is, $\mathbb{E}[||\mathbf{s} - \mathbf{W}^{\mathsf{H}}\mathbf{y}_r||_2^2] = \mathrm{tr}(\mathbb{E}[\mathbf{ss}^{\mathsf{H}}]) - 2\mathbb{R}\{\mathrm{tr}(\mathbb{E}[\mathbf{sy}_r^{\mathsf{H}}]\mathbf{W})\} + \mathrm{tr}(\mathbf{W}^{\mathsf{H}}\mathbb{E}[\mathbf{y}_r\mathbf{y}_r^{\mathsf{H}}]\mathbf{W}).$

Remark 5. It is important to note that the design of the combiners relies on the decoupling of the precoding and combining processes as we have assumed fixed optimal precoders $(\mathbf{F}_{\mathrm{F}}^{\mathrm{opt}}, \mathbf{F}_{B}^{\mathrm{opt}})$. Although this decoupling decreases the complexity involved in the design of practical mmWave precoders and combiners with transceiver RTHIs, care must be taken as oversimplification can lead to received power losses. A precaution to note will be addressed afterward.

To this end, we introduce a term independent of the combiners, that is, $\mathrm{tr}(\mathbf{W}_M^{\mathsf{H}}\mathbb{E}[\mathbf{y}_r\mathbf{y}_r^{\mathsf{H}}\mathbf{W}_M]) - \mathrm{tr}(\mathbb{E}[\mathbf{ss}^{\mathsf{H}}])$, where $\mathbf{W}_M$ is the common conventional solution to the unconstrained MMSE problems described by

$$\mathbf{W}_M^{\mathsf{H}} = \mathbb{E}[\mathbf{sy}_r^{\mathsf{H}}]\mathbb{E}[\mathbf{y}_r\mathbf{y}_r^{\mathsf{H}}]^{-1}. \quad (35)$$

Using $\mathbf{y}_r$ in (1), we obtain

$$\mathbf{W}_M^{\mathsf{H}} = \frac{1}{\sqrt{\rho}}\left(\mathbf{F}^{\mathsf{H}}\mathbf{H}^{\mathsf{H}}\mathbf{HF} + \frac{\sigma^2 M_s}{\rho}\mathbf{I}_{M_s}\right)^{-1}\mathbf{F}^{\mathsf{H}}\mathbf{H}^{\mathsf{H}}. \quad (36)$$

Denoting the objective function of (34) as $\mathcal{I}(\mathbf{W})$ and including the independent term $\mathrm{tr}(\mathbf{W}_M^{\mathsf{H}}\mathbb{E}[\mathbf{y}_r\mathbf{y}_r^{\mathsf{H}}\mathbf{W}_M]) - \mathrm{tr}(\mathbb{E}[\mathbf{ss}^{\mathsf{H}}])$, the function takes the form

$$\mathcal{I}(\mathbf{W}) = \mathrm{tr}\left(\mathbf{W}_M^{\mathsf{H}}\mathbb{E}[\mathbf{y}_r\mathbf{y}_r^{\mathsf{H}}\mathbf{W}_M]\right) - \mathrm{tr}\left(\mathbb{E}[\mathbf{ss}^{\mathsf{H}}]\right)$$
$$+ \mathrm{tr}\left(\mathbb{E}[\mathbf{ss}^{\mathsf{H}}]\right) - 2\mathbb{R}\left\{\mathrm{tr}\left(\mathbb{E}[\mathbf{sy}_r^{\mathsf{H}}]\mathbf{W}\right)\right\} \quad (37)$$
$$+ \mathrm{tr}\left(\mathbf{W}^{\mathsf{H}}\mathbb{E}[\mathbf{y}_r\mathbf{y}_r^{\mathsf{H}}]\mathbf{W}\right).$$

Given that $\mathbb{E}[\mathbf{sy}_r^{\mathsf{H}}] = \mathbf{W}_M^{\mathsf{H}}\mathbb{E}[\mathbf{y}_r\mathbf{y}_r]$ from (35), and having in mind the equivalence of $\mathrm{tr}(\mathbb{E}[\mathbf{sy}_r^{\mathsf{H}}]\mathbf{W})$ and $\mathrm{tr}(\mathbb{E}[\mathbf{sy}_r^{\mathsf{H}}]\mathbb{E}[\mathbf{y}_r\mathbf{y}_r^{\mathsf{H}}]\mathbb{E}[\mathbf{y}_r\mathbf{y}_r^{\mathsf{H}}]^{-1}\mathbf{W})$, (37) becomes

$$\mathcal{I}(\mathbf{W}) = \mathrm{tr}\left(\mathbf{W}_M^{\mathsf{H}}\mathbb{E}[\mathbf{y}_r\mathbf{y}_r^{\mathsf{H}}\mathbf{W}_M]\right) \quad (38)$$
$$-2\mathbb{R}\{\mathrm{tr}(\mathbb{E}[\mathbf{W}_M^{\mathsf{H}}\mathbb{E}[\mathbf{y}_r\mathbf{y}_r]\mathbf{W}])\} + \mathrm{tr}(\mathbf{W}^{\mathsf{H}}\mathbb{E}[\mathbf{y}_r\mathbf{y}_r^{\mathsf{H}}]\mathbf{W})$$
$$= \mathrm{tr}\left((\mathbf{W}_M^{\mathsf{H}} - \mathbf{W}^{\mathsf{H}})\mathbb{E}[\mathbf{y}_r\mathbf{y}_r^{\mathsf{H}}](\mathbf{W}_M - \mathbf{W})\right)$$
$$\overset{(a)}{=} ||\mathbb{E}[\mathbf{y}_r\mathbf{y}_r^{\mathsf{H}}]^{1/2}(\mathbf{W}_M - \mathbf{W})||_F^2, \quad (39)$$

where (*a*) follows from the definition of the Frobenius norm. Due to (38), the optimization problem becomes

$$\mathcal{R}_2 : (\mathbf{W}_{\mathrm{F}}^{\mathrm{opt}}, \mathbf{W}_{\mathrm{B}}^{\mathrm{opt}}) = \underset{\mathbf{W}_{\mathrm{F}}, \mathbf{W}_{\mathrm{B}}}{\arg\min}|| \mathbb{E}[\mathbf{y}_r\mathbf{y}_r^{\mathsf{H}}]^{1/2}(\mathbf{W}_M - \mathbf{W})||_F,$$
$$\text{s.t. } \mathbf{W}_{\mathrm{F}} \in \mathcal{W}_{\mathrm{F}}. \quad (40)$$

In other words, we aim to find the projection of the combiner (having no constraints) $\mathbf{W}_M$ onto the set of combiners (by means of the weighted $\mathbb{E}[\mathbf{y}_r\mathbf{y}_r^{\mathsf{H}}]$) having the form $\mathbf{W} = \mathbf{W}_{\mathrm{F}}\mathbf{W}_{\mathrm{B}}$ with $\mathbf{W}_{\mathrm{F}}$ existing in a set of $\mathcal{W}_{\mathrm{F}}$. Comparable to the design of the optimal precoders in Section 4, it is algorithmically intractable to find this projection in closed form due to the non-convexity of the set $\mathcal{W}_{\mathrm{F}}$. Accordingly, we exploit the aforementioned properties of the mmWave MIMO channel to result in a near-optimal solution to (40). Specifically, an orthonormal basis is formed for the columns of $\mathbf{W}_{\mathrm{F}}$ by the linearly independent array response vectors, $\mathbf{a}_r(\boldsymbol{\phi}_l)$ so that the receiver utilizes N^{F} of the vectors $\mathbf{a}_r(\boldsymbol{\phi}_l)$ at the RF using analog phase shifters.

For this reason, we can rewrite the optimization problem $\mathcal{R}_2$ by restricting the columns of $\mathbf{W}_{\mathrm{F}}$ to have the form of $\mathbf{a}_r(\boldsymbol{\phi}_l)$ as follows

$$\mathcal{R}_3 : (\mathbf{W}_{\mathrm{F}}^{\mathrm{opt}}, \mathbf{W}_{\mathrm{B}}^{\mathrm{opt}}) = \underset{\mathbf{W}_{\mathrm{F}}, \mathbf{W}_{\mathrm{B}}}{\arg\min}|| \mathbb{E}[\mathbf{y}_r\mathbf{y}_r^{\mathsf{H}}]^{1/2}(\mathbf{W}_M - \mathbf{W})||_F,$$
$$\text{s.t. } \mathbf{W}_{\mathrm{F}}^{(l)} \in \{\mathbf{a}_r(\boldsymbol{\phi}_l), \ \forall l\}. \quad (41)$$

Herein, the task is to find the optimal combiner in terms of the optimal basis formed by $\mathbf{a}_r(\boldsymbol{\phi}_l)$. Moreover, by inserting $\mathbf{W}_{\mathrm{F}}^{(l)}$ into the objective function results in $\mathcal{R}_4$ providing $\mathbf{W}_{\mathrm{B}}^{\mathrm{opt}}$ as

$$\mathcal{R}_4 : (\widetilde{\mathbf{W}}_{\mathrm{B}}^{\mathrm{opt}})$$
$$= \underset{\widetilde{\mathbf{W}}_{\mathrm{B}}}{\arg\min} || \mathbb{E}[\mathbf{y}_r\mathbf{y}_r^{\mathsf{H}}]^{\frac{1}{2}}\mathbf{W}_M - \mathbb{E}[\mathbf{y}_r\mathbf{y}_r^{\mathsf{H}}]^{\frac{1}{2}}\mathbf{A}_r\widetilde{\mathbf{W}}_{\mathrm{B}}||_F,$$
$$\text{s.t. } || \mathrm{diag}(\widetilde{\mathbf{W}}_{\mathrm{B}}\widetilde{\mathbf{W}}_{\mathrm{B}}^{\mathsf{H}})||_0 = N^{\mathrm{F}}, \quad (42)$$

where $\mathbf{A}_r = [\mathbf{a}_r(\boldsymbol{\phi}_1), \dots, \mathbf{a}_r(\boldsymbol{\phi}_L)]$ is an $N \times L$ matrix that includes the array response vectors, and $\widetilde{\mathbf{W}}_{\mathrm{B}}$ is an $L \times M_s$ matrix.

The solution of the optimization problem, delineated by $\mathcal{R}_4$, can be obtained by means of the modified OMP method presented in Section 4. Hence, Algorithm 2 results in the solution of the combiner while having first found the vector $\mathbf{a}_r(\boldsymbol{\phi}_l)$ and then designed N^{F} beamforming vectors to express the optimal $\mathbf{W}_{\mathrm{F}}^{\mathrm{opt}}$. Having determined $\mathbf{W}_{\mathrm{F}}$, the calculation of the optimal $\mathbf{W}_{\mathrm{B}}$ is achieved at Step 8.

As already mentioned, it is imperative to avoid any oversimplification of the practical mmWave MIMO transceiver design with RTHIs as this can lead to losses in the received power. To avoid this, it becomes pertinent to start the design with the more constrained side of the mmWave MIMO system. In other words, the algorithms presented do not have to be carried out

ALGORITHM 2 Spatially Sparse Combining with RATHIs by OMP

1   **Require** $\mathbf{W}_M$

2    $\mathbf{W}_F$ = Empty Matrix

3    $\mathbf{W}_{res} = \mathbf{W}_M$

4   **for** $i \leq N^F$ **do**

5       $\mathbf{\Psi} = \mathbf{A}_r^H \mathbb{E}[\mathbf{y}_r \mathbf{y}_r^H] \mathbf{W}_{res}$

6       $k = \underset{l=1,\dots,L}{\arg\max} \, (\mathbf{\Psi}\mathbf{\Psi}^H)_{l,l}$

7       $\mathbf{W}_F = \left[\mathbf{W}_F | \mathbf{A}_r^{(k)} \right]$

8       $\mathbf{W}_B = \left(\mathbf{W}_F^H \mathbb{E}[\mathbf{y}_r \mathbf{y}_r^H] \mathbf{W}_F \right)^{-1} \mathbf{W}_F^H \mathbb{E}\left[\mathbf{y}_r \mathbf{y}_r^H \right] \mathbf{W}_M$

9       $\mathbf{W}_{res} = \frac{\mathbf{W}_M - \mathbf{W}_F \mathbf{W}_B}{||\mathbf{W}_M - \mathbf{W}_F \mathbf{W}_B||_F}$

10   **end**

11   **return** $\mathbf{W}_F, \mathbf{W}_B$

TABLE 1 Simulation Parameters

Notation	Parameter	Values
M	Number of transmit antennas	64
N	Number of receive antennas	64
σ^2	Thermal noise variance	−174 dbm/Hz
M_s	Number of transmit streams	3
M^F	Number of transmit RF chains	4
N^F	Number of receive RF chains	4

in succession. In fact, a rule of thumb to achieve minimal losses in the design is to compare the number of RF chains at both the transmitter and receiver of the mmWave system. The smaller of the two indicates which side is more constrained and the design must begin from there. For example, if $M^F < N^F$, then the design should start with Algorithm 1 to find the optimal precoders before going on to determine the optimal combiners by means of Algorithm 2. The converse would be applicable if $M^F > N^F$, and such design would begin with designing the combiners first. In this case, since Algorithm 2 assumes fixed precoders, we apply the assumption that $\mathbf{F} = \widetilde{\mathbf{V}}_1$. Having found the optimal combiners, an effective channel ($\mathbf{W}^H \mathbf{H}$) is formed and then we apply SVD to obtain the equivalent unitary and diagonal matrices, that is, $\mathbf{W}^H \mathbf{H} = \mathbf{U} \mathbf{\Sigma} \mathbf{V}^H$. Finally, Algorithm 1 can be used to obtain the optimal precoders using the new $\mathbf{V}$.

5 | NUMERICAL RESULTS

In this section, we depict the analytical results, and particularly, *the impact of the RTHIs to the SE given by* (28). Notably, we verify the mathematical expressions by simulations, and we depict the impact of the various RTHIs on the SE, provided by (12). The simulation parameters, presented in Table 1, are inspired by related studies on non-ideal hardware and mmWave MIMO wireless communications [10, 19]. Especially, the selection of the nominal values for the RTHIs is based on the correspond-

FIGURE 2 SE versus the SNR in a 64×64 mmWave MIMO system depicting the effect of RATHIs

ing values for systems operating in sub-6 GHz frequency bands since no such values exist for systems in the mmWave range. However, our results achieve to shed light on the impact of RTHIs on mmWave systems with hybrid precoding. However, since it is expected that mmWave communication will rely on massive MIMO systems, the values of RTHIs that have been used in this work correspond to the values that will be met in mmWave transmissions. The values of all other parameters will be provided during their use. Specifically, let a transmitter communicate through multiple channel streams to the receiver by 8 clusters and 10 rays per cluster. The distributions of the azimuth and elevation angles of arrival (AoAs) and departure (AoDs) follow Laplacian probability density function having an angular spread of 7.5°. We assume equal transmit power ρ in all precoding and combining solutions. Basically, we will employ $\bar{\rho}$ expressing the signal to noise ratio, that is, SNR = $\bar{\rho}$. The ATN follows the Gaussian distribution. Our objective is to examine the impact of each hardware impairment separately, as shown below.

5.1 | Evaluation of RATHIs

In Figures 2 and 3, we focus on how the RATHIs affect the SE by neglecting the impact of ATN. Specifically, in Figure 2, we present the SE versus the SNR by varying the RATHIs, that is, by varying κ_t^2 and κ_r^2, respectively. In particular, we have not selected arbitrary values, but values adopted from system measurements in [19]. We observe the negligible effect of the RATHIs at low SNRs, which means below 0 dB since the saturation of the SE with comparison to the ideal case starts later. Especially, when SNR > 0 dB, the degradation of SE increases with more severe RATHIs in terms of κ_t^2 and κ_r^2. This is a very interesting result for mmWave systems implying that the RATHIs will have a small effect on their performance since mmWave communications are basically identified by
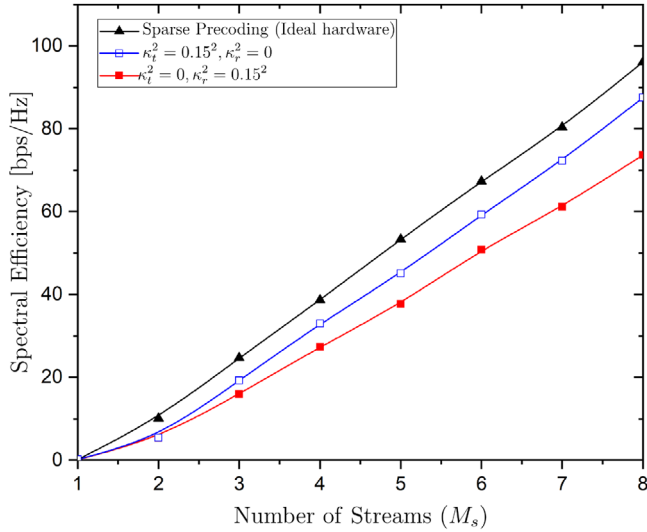
FIGURE 3 SE versus the number of streams in a 64 × 64 mmWave MIMO system depicting the effect of RATHIs

FIGURE 4 SE versus the SNR in a 64 × 64 mmWave MIMO system depicting the effect of ATN

transmission in the low SNR regime. Another important observation in Figure 2 shows that the receiver distortion impairments contribute a higher amount of degradation to the SE than the transmitter impairments. As illustrated in the figure, for an SNR of 0 dB, when we set $\kappa_r^2 = 0$ and $\kappa_t^2 = 0.15^2$, the SE is degraded by about 10 bps/Hz whereas when $\kappa_t^2 = 0$ and $\kappa_r^2 = 0.15^2$, the SE is degraded by 12 bps/Hz. This observation is quite interesting and useful. It suggests that in the case of communication at the high SNR regime, a possible design scheme could be to keep κ_t^2 constant and varying the quality of receiver hardware in order to achieve the desired SE. Moreover, in the case of better quality hardware, the degradation is lower as can be seen, for example, when $\kappa_r^2 = 0$ and $\kappa_t^2 = 0.08^2$.

Figure 3 depicts the variation of the RATHIs with respect to the number of streams. From the figure, it can be seen that an increase in the number of streams M_s above 3 yields a different degradation of the SE for κ_t^2 and κ_r^2. Especially, the impact of the transmitter distortions on the system stays constant, yielding a decrease in SE from the ideal case of about 8 bps/Hz while the decrease in the SE due to receiver distortions starts from about 10 bps/Hz and increases. In addition, it can be observed that for a lower number of streams, that is, $M_s = 1, 2$, the receive and transmitter distortions contribute almost the same to the degradation to the SE. This result is specifically important for the design considerations of mmWave systems and validates the suggestion in the literature that the increase in the number of streams improves the accuracy of hybrid precoding schemes.

5.2 | Evaluation of ATN

In order to show the impact of ATN on the SE, we assume that RATHIs have no impact. Hence, we illustrate the SE versus the SNR by varying σ_ξ^2 based on measurements [19]. In particular, in
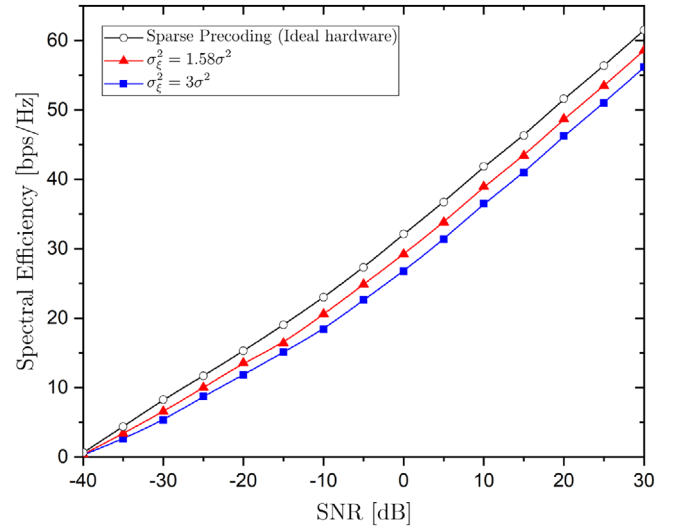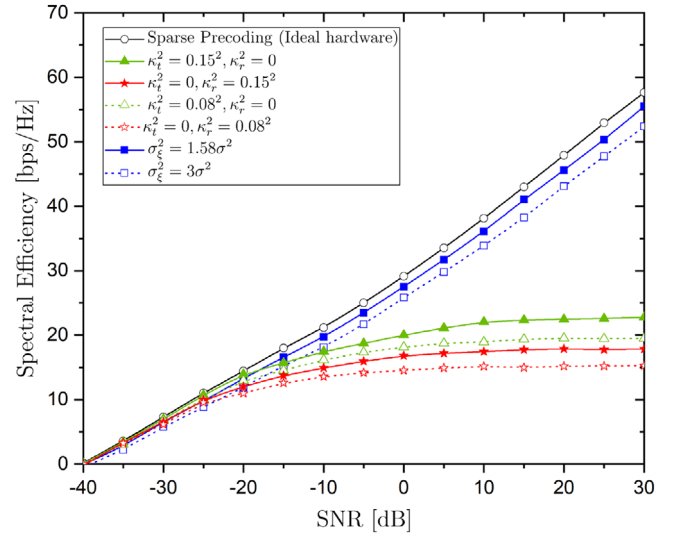

FIGURE 5 Comparison of the SE versus SNR in a 64 × 64 mmWave MIMO system depicting in the same figure the effect of RATHIs and ATN

Figure 4, we observe a constant degradation in SE for all SNRs, which worsens with increasing σ_ξ^2. As a result, the ATN should be taken into account in the design of mmWave communication systems.

Figure 5 presents a comparison of the SE performance by using ideal hardware versus imperfect hardware with $(\kappa_t^2 = 0, \kappa_r^2 = 0.15^2)$, $(\kappa_t^2 = 0.15^2, \kappa_r^2 = 0)$, $(\kappa_t^2 = 0, \kappa_r^2 = 0.08^2)$, $(\kappa_t^2 = 0.08^2, \kappa_r^2 = 0)$, $\sigma_\xi^2 = 1.5\sigma^2$, and $\sigma_\xi^2 = 3\sigma^2$. These baseline hardware imperfection values differ by the same ratio, in other words, the two corresponding values of RATHIs and ATN have the same ratio of $\frac{1}{2}$. It can be observed from the figure that ATN increases monotonically with the SNR. Evidently, receiver distortions have the greatest impact causing the
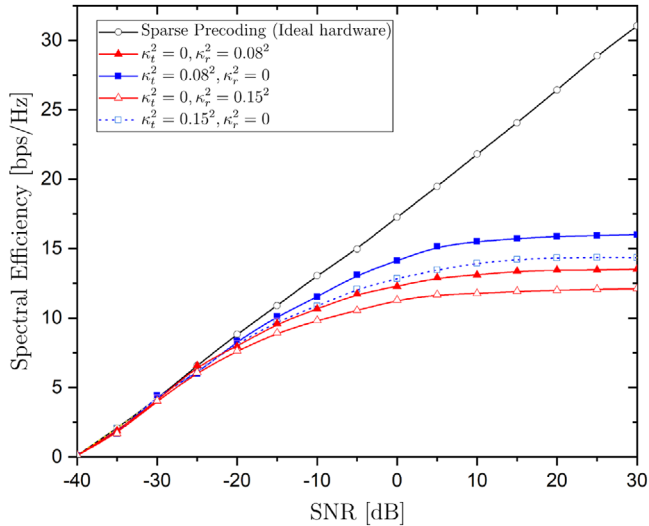
FIGURE 6 SE versus the SNR in a 64×32 mmWave MIMO system depicting the effect of RATHIs

most degradation in SE when compared with the performance using ideal hardware. Notably, when comparing the degradation between each separate impairment for a given specific ratio at low SNR, ATN performs the worst until -15 dB. However, at higher SNR values, RATHIs become more severe.

Figure 6 relies on similar settings as Figure 2 but contrary to previous figures that assume $M = N$, it shows the SE performance for $M = 32$ and $N = 64$. Hence, compared to 2, we observe that a variation of M from 64 to 32 affects the SE. However, in the case of variation of N, the SE does not change. These properties can also be observed by means of the SE expression given by (28). Shedding further light, we notice that the SE decreases when M decreases. Also, although RATHIS result in SE saturation, they have a weaker impact on the performance. For example, for an SNR of 0 dB, when we set $\kappa_r^2 = 0$ and $\kappa_t^2 = 0.15^2$, SE is degraded by about 4 bps/Hz whereas when $\kappa_t^2 = 0$ and $\kappa_r^2 = 0.15^2$, SE is degraded by 6 bps/Hz, which are lower compared to Figure 2.

6 | CONCLUSION

Hybrid processing (precoding/combining) solutions are prominent in mmWave MIMO communication as they provide a balance between cost, complexity, and system performance in terms of SE. Even though RTHIs are unavoidable in a communication system, their effects have not been adequately taken into account in mmWave systems with hybrid precoding as prior studies with hybrid precoding have assumed perfect hardware. Hence, the aim of this paper was to examine the effect of RTHIs on mmWave MIMO systems with hybrid precoding. In particular, we provided a full analysis of the impact of RATHIs and ATN on the performance of a hybrid precoding system operating in mmWave frequency bands. Therefore, we considered realistic hardware impairment values from the related lit-

erature and observed their impact on the SE. The outcomes revealed that the receiver distortions degrade the system performance more, than the transmitter distortions. Moreover, the ATN, which causes a constant degradation to the SE, becomes increasingly critical for higher values of its variance at the low SNR regime. Furthermore, we examined how the key system parameters, such as the number of streams, affect the impact of RATHIs. Remarkably, among other observations, we noted that an increase in the number of streams increases the impact of the receiver additive distortion. Also, mmWave systems with low SNR communication are not susceptible to RATHIs which become more severe if we select transmission at higher SNR. These observations could be considered among others as design options to improve the SE of realistic mmWave MIMO systems with hybrid precoding and unavoidable RTHIs.

PERMISSION TO REPRODUCE MATERIALS FROM OTHER SOURCES

None

ORCID

Anastasios K. Papazafeiropoulos https://orcid.org/0000-0003-1841-6461

REFERENCES

1. Andrews, J.G., et al.: What will 5G be? IEEE J. Sel. Areas Commun. 32(6), 1065–1082 (2014)
2. Pi, Z., Khan, F.: An introduction to millimeter-wave mobile broadband systems. IEEE Commun. Mag. 49(6), 101–107 (2011)
3. Rappaport, T.S., et al.: Millimeter wave mobile communications for 5G cellular: It will work! IEEE Access 1, 335–349 (2013)
4. Alkhateeb, A., et al.: MIMO precoding and combining solutions for millimeter-wave systems. IEEE Commun. Mag. 52(12), 122–131 (2014)
5. Alkhateeb, A., et al.: Limited feedback hybrid precoding for multi-user millimeter wave systems. IEEE Trans. Wireless Commun. 14(11), 6481–6494 (2015)
6. Andrews, J.G., et al.: Modeling and analyzing millimeter wave cellular systems. IEEE Trans. Commun. 65(1), 403–430 (2017)
7. Kulkarni, M.N., et al.: A comparison of MIMO techniques in downlink millimeter wave cellular networks with hybrid beamforming. IEEE Trans. Commun. 64(5), 1952–1967 (2016)
8. Magueta, R., et al.: Hybrid multi-user equalizer for massive MIMO millimeter-wave dynamic subconnected architecture. IEEE Access 7, 79017–79029 (2019)
9. Han, S., et al.: Large-scale antenna systems with hybrid analog and digital beamforming for millimeter wave 5G. IEEE Commun. Mag. 53(1), 186–194 (2015)
10. Ayach, O.E., et al.: Spatially sparse precoding in millimeter wave MIMO systems. IEEE Trans. Wireless Commun. 13(3), 1499–1513 (2014)
11. Alkhateeb, A., et al.: Achievable rates of multi-user millimeter wave systems with hybrid precoding. In: IEEE International Conference on Communication Workshop (ICCW), pp. 1232–1237. IEEE, Piscataway (2015)

12. Teodoro, S., et al.: Theoretical analysis of nonlinear amplification effects in massive MIMO systems. IEEE Access 7, 172277–172289 (2019)

13. X. Xue, et al.: Energy-efficient hybrid precoding for massive MIMO mmWave systems with a fully-adaptive-connected structure. IEEE Trans. Commun. 68(6), 3521–3535 (2020)

14. Elbir, A.M., Papazafeiropoulos, A.K.: Hybrid precoding for multiuser millimeter wave massive MIMO systems: A deep learning approach. IEEE Trans. Veh. Tech. 69(1), 552–563 (2020)

15. Schenk, T.: RF Imperfections in High-Rate Wireless Systems: Impact and Digital Compensation. Springer Science & Business Media, Dordrecht (2008)

16. Studer, C., et al.: MIMO transmission with residual transmit-RF impairments. In: International ITG Workshop on Smart Antennas (WSA), pp. 189–196. IEEE, Piscataway (2010)

17. Qi, J., Aissa, S.: Analysis and compensation of power amplifier nonlinearity in MIMO transmit diversity systems. IEEE Trans. Veh. Tech. 59(6), 2921–2931 (2010)

18. Zetterberg, P.: Experimental investigation of TDD reciprocity-based zero-forcing transmit precoding. EURASIP J. Advances Signal Process. 2011, 1–10 (2011)

19. Björnson, E., et al.: Massive MIMO systems with non-ideal hardware: Energy efficiency, estimation, and capacity limits. IEEE Trans. Inf. Theory 60(11), 7112–7139 (2014)

20. Björnson, E., et al.: Massive MIMO with non-ideal arbitrary arrays: Hardware scaling laws and circuit-aware design. IEEE Trans. Wireless Commun. 14(8), 4353–4368 (2015)

21. Zhang, X., et al.: On the MIMO capacity with residual transceiver hardware impairments. In: IEEE International Conference on Communications (ICC), pp. 5299–5305. IEEE, Piscataway (2014)

22. Gustavsson, U., et al.: On the impact of hardware impairments on massive MIMO. In: IEEE Globecom Workshops (GC Wkshps), pp. 294–300. IEEE, Piscataway (2014)

23. Athley, F., et al.: Analysis of massive MIMO with hardware impairments and different channel models. In: 29th European Conference on Antennas and Propagation (EuCAP), pp. 1–5. IEEE, Piscataway (2015)

24. Papazafeiropoulos, A.K., Ratnarajah, T.: Downlink MIMO HCNs with residual transceiver hardware impairments. IEEE Commun. Lett. 20(10), 2023–2026 (2016)

25. Zhu, J., et al.: Analysis and design of secure massive MIMO systems in the presence of hardware impairments. IEEE Trans. Wireless Commun. 16(3), 2001–2016 (2017)

26. Papazafeiropoulos, A.K.: Impact of general channel aging conditions on the downlink performance of massive MIMO. IEEE Trans. Veh. Tech. 66(2), 1428–1442 (2017)

27. Papazafeiropoulos, A., Ratnarajah, T.: Towards a realistic assessment of multiple antenna HCNs: Residual additive transceiver hardware impairments and channel aging. IEEE Trans. Veh. Tech. 66(10), 9061–9073 (2017)

28. Papazafeiropoulos, A., et al.: Rate-splitting to mitigate residual transceiver hardware impairments in massive MIMO systems. IEEE Trans. Veh. Tech. 66(9), 8196–8211 (2017)

29. Papazafeiropoulos, A., et al.: Ergodic capacity analysis of amplify-and-forward dual-hop MIMO relay systems with residual transceiver hardware impairments: Conventional and large system limits. IEEE Trans. Veh. Tech. 66(8), 7010–7025 (2017)

30. Papazafeiropoulos, A., et al.: Impact of residual additive transceiver hardware impairments on Rayleigh-product MIMO channels with linear receivers: Exact and asymptotic analyses. IEEE Trans. Commun. 66(1), 105–118 (2018)

31. Gimenez, S., et al.: Performance evaluation of analog beamforming with hardware impairments for mmW massive MIMO communication in an urban scenario. IEEE Sensors J. 16(10), 1555 (2016)

32. Zou, Y., et al.: Impact of major RF impairments on mm-wave communications using OFDM waveforms. In: IEEE Globecom Workshops (GC Wkshps), pp. 1–7. IEEE, Piscataway (2016)

33. Papazafeiropoulos, A., et al.: Nuts and bolts of a realistic stochastic geometric analysis of mmWave HetNets: Hardware impairments and channel aging. IEEE Trans. Veh. Tech. 68(6), 5657–5671 (2019)

34. Papazafeiropoulos, A.: Impact of hardware impairments and channel aging millimeter-wave heterogeneous networks. In: IEEE Wireless Communications and Networking Conference (WCNC), pp. 1–7. IEEE, Piscataway (2019)

35. Kolawole, O.Y., et al.: Impact of hardware impairments on mmwave MIMO systems with hybrid precoding. In: 2018 IEEE Wireless Communications and Networking Conference (WCNC), pp. 1–6. IEEE, Piscataway (2018)

36. Tropp, J.A., Gilbert, A.C.: Signal recovery from random measurements via orthogonal matching pursuit. IEEE Trans. Inf. Theory 53(12), 4655–4666 (2007)

37. Torkildson, E., et al.: Millimeter-wave spatial multiplexing in an indoor environment. In: IEEE Globecom Workshops, pp. 1–6. IEEE, Piscataway (2009)

38. Goldsmith, A., et al.: Capacity limits of MIMO channels. IEEE J. Sel. Areas Commun. 21(5), 684–702 (2003)

39. Smulders, P., Correia, L.: Characterisation of propagation in 60 GHz radio channels. Electron. Commun. Eng. J. 9(2), 73–80 (1997)

40. Xu, H., et al.: Spatial and temporal characteristics of 60-GHz indoor channels. IEEE J. Sel. Areas Commun. 20(3), 620–630 (2002)

41. Holma, H., Toskala, A.: LTE for UMTS: Evolution to LTE-Advanced. John Wiley & Sons, Chichester (2011)

42. Palomar, D.P., et al.: Joint Tx-Rx beamforming design for multicarrier MIMO channels: A unified framework for convex optimization. IEEE Trans. Signal Process. 51(9), 2381–2401 (2003)

43. Bauschke, H.H., Borwein, J.M.: On projection algorithms for solving convex feasibility problems. SIAM Rev. 38(3), 367–426 (1996)

44. Escalante, R., Raydan, M.: Alternating Projection Methods, vol. 8. SIAM, Philadelphia (2011)

45. Pati, Y.C., et al.: Orthogonal matching pursuit: Recursive function approximation with applications to wavelet decomposition. In: Proceedings of 27th Asilomar Conference on Signals, Systems and Computers, vol. 1, pp. 40–44. IEEE, Piscataway (1993)

46. Rebollo-Neira, L., Lowe, D.: Optimized orthogonal matching pursuit approach. IEEE Signal Process. Lett. 9(4), 137–140 (2002)

47. Kailath, T., et al.: Linear Estimation, vol. 1. Prentice Hall, Upper Saddle River (2000)

48. Michaeli, T., Eldar, C.Y.: Constrained linear minimum MSE estimation. https://webee.technion.ac.li/uploads/file/publication/641.pdf, 2007.

APPENDIX A: PROOF OF LEMMA 1

The SE is obtained by means of (9) based on the covariance matrix of the additive noise **e**, which is given by

$$
\mathbf{R}_e = \mathbb{E}\{(\mathbf{H}\boldsymbol{\eta}_t + \boldsymbol{\eta}_r + \boldsymbol{\xi})(\mathbf{H}\boldsymbol{\eta}_t + \boldsymbol{\eta}_r + \boldsymbol{\xi})^{\mathsf{H}}\}
$$

$$
\overset{(a)}{=} \mathbf{H}\mathbb{E}\{\boldsymbol{\eta}_t\boldsymbol{\eta}_t^{\mathsf{H}}\}\mathbf{H}^{\mathsf{H}} + \mathbb{E}\{\boldsymbol{\eta}_r\boldsymbol{\eta}_r^{\mathsf{H}}\} + \mathbb{E}\{\boldsymbol{\xi}\boldsymbol{\xi}^{\mathsf{H}}\}
$$

$$
\overset{(b)}{=} \frac{\kappa_t^2 \rho}{M_s}\mathbf{H}\mathbf{H}^{\mathsf{H}} + \kappa_r^2 \rho \mathbf{H}\mathbf{H}^{\mathsf{H}} + \sigma_{\xi}^2 \mathbf{I}_N, \tag{43}
$$

where (a) is due to the statistical independence of each random variable with the rest, and (b) is due to (10) and (11).

APPENDIX B: ANALYSIS FOR THE CASE WHERE $N < M$

In this case, the partition for the matrix with the singular values is given by

$$\Sigma = \begin{bmatrix} \Sigma_1 & \mathbf{O}_{M_s,K'} & \mathbf{O}_{M_s,L'} \\ \mathbf{O}_{K',M_s} & \Sigma_2 & \mathbf{O}_{K',L'} \end{bmatrix}, \tag{44}$$

where $L' = M - N$ and $K' = N - M_s$. From (17), we now obtain

$$\mathbf{D} = \begin{bmatrix} \mathbf{D}_1 & \mathbf{O}_{M_s,K'} \\ \mathbf{O}_{K',M_s} & \mathbf{D}_2 \end{bmatrix}$$

$$= \begin{bmatrix} \beta\Sigma_1^2 + \sigma_\xi^2 \mathbf{I}_{M_s} & \mathbf{O}_{M_s,K'} \\ \mathbf{O}_{K',M_s} & \beta\Sigma_2^2 + \sigma_\xi^2 \mathbf{I}_{K'} \end{bmatrix}. \tag{45}$$

Following a similar approach, the matrix $\mathbf{B}$ equals

$$\mathbf{B} = \frac{\rho}{M_s}\Sigma^T \mathbf{D}^{-1}\Sigma$$

$$= \begin{bmatrix} \mathbf{B}_1 & \mathbf{O}_{M_s,K} \\ \mathbf{O}_{K,M_s} & \mathbf{B}_2 \end{bmatrix}, \tag{46}$$

where $\mathbf{B}_1$ is given by (24) and

$$\mathbf{B}_2 = \begin{bmatrix} \frac{\rho}{M_s}\Sigma_2^2 \mathbf{D}_2^{-1} & \mathbf{O}_{K',L'} \\ \mathbf{O}_{L',K'} & \mathbf{O}_{L',L'} \end{bmatrix} \in \mathbb{C}^{K \times K}. \tag{47}$$

Thus, by substituting (47) and (24) into (18) we can derive (26) for the case where $N < M$ by following a similar approach regarding the analysis.